RESEARCH ARTICLE

ISEV

An extracellular vesicular mutant KRAS-associated protein complex promotes lung inflammation and tumor growth

Mukesh K. Sriwastva[1] | **Yun Teng[1]** | **Jingyao Mu[1]** | **Fangyi Xu[1]** | **Anil Kumar[1]** | **Kumaran Sundaram[1]** | **Rajiv Kumar Malhotra[1]** | **Qingbo Xu[1]** | **Joshua L. Hood[2]** | **Lifeng Zhang[1]** | **Jun Yan[1]** | **Michael L. Merchant[3]** | **Juw Won Park[4,5]** | **Gerald W. Dryden[1,5,2]** | **Nejat K. Egilmez[1]** | **Huang-Ge Zhang[1,6]**

[1]Brown Cancer Center, Department of Microbiology & Immunology, University of Louisville, Louisville, Kentucky, USA

[2]Department of Pharmacology and Toxicology, University of Louisville, Louisville, Kentucky, USA

[3]Kidney Disease Program and Clinical Proteomics Center, University of Louisville, Louisville, Kentucky, USA

[4]KBRIN Bioinformatics Core, University of Louisville, Louisville, Kentucky, USA

[5]Department of Computer Engineering and Computer Science, University of Louisville, Louisville, Kentucky, USA

[6]Robley Rex Veterans Affairs Medical Center, Louisville, Kentucky, USA

Correspondence
Yun Teng and Huang-Ge Zhang, James Graham Brown Cancer Center, University of Louisville, CTRB 309, 505 Hancock Street, Louisville, KY 40202, USA.
Email: h0zhan17@louisville.edu and yun.teng@louisville.edu

Abstract
Extracellular vesicles (EVs) contain more than 100 proteins. Whether there are EVs proteins that act as an 'organiser' of protein networks to generate a new or different biological effect from that identified in EV-producing cells has never been demonstrated. Here, as a proof-of-concept, we demonstrate that EV-G12D-mutant KRAS serves as a leader that forms a protein complex and promotes lung inflammation and tumour growth via the Fn1/IL-17A/FGF21 axis. Mechanistically, in contrast to cytosol derived G12D-mutant KRAS complex from EVs-producing cells, EV-G12D-mutant KRAS interacts with a group of extracellular vesicular factors via fibronectin-1 (Fn1), which drives the activation of the IL-17A/FGF21 inflammation pathway in EV recipient cells. We show that: (i), depletion of EV-Fn1 leads to a reduction of a number of inflammatory cytokines including IL-17A; (ii) induction of IL-17A promotes lung inflammation, which in turn leads to IL-17A mediated induction of FGF21 in the lung; and (iii) EV-G12D-mutant KRAS complex mediated lung inflammation is abrogated in IL-17 receptor KO mice. These findings establish a new concept in EV function with potential implications for novel therapeutic interventions in EV-mediated disease processes.

KEYWORDS
extracellular vesicles (EV), fibronectin (Fn1), inflammation, KRAS, lung tumour, plant lipid liposomes, Protein networks

1 | INTRODUCTION

Extracellular vesicles (EVs) are nano-sized vesicles released from different types of cells. The EVs have been recognised as intercellular communicators (Kalluri & LeBleu, 2020). EV cargo is transferred from a donor cell to a recipient cell, leading to changes

in gene expression and cell function in health and disease (Buzas et al., 2014; Kharaziha et al., 2012; Masyuk et al., 2013; Sriwastva et al., 2022; Teng et al., 2018). However, whether the molecule(s) in EVs have the same function in recipient cells as in the EV donor cells is largely unknown. Moreover, the structural mechanics of EV protein activity in recipient cells, that is, either as individual molecules or as functionally superior multi-protein complexes, has not been examined. Filling in this key gap in our current knowledge would further clarify the molecular basis of the unique biological effects mediated by EVs on the recipient cell and add to the current conceptual framework of EV biology.

The EV microenvironment is different from the microenvironment of the EV-producing cell. There is an obvious size difference in EVs compared to the EV-producing cells. Protein-protein interaction is determined by a number of factors including proximity (Deng et al., 2012, Larochelle et al., 2019, Liu et al., 2018, To et al., 2014, Zheng et al., 2019). The proximity of proteins for protein-protein interaction is expected to be closer within EVs than within the cytosol of EV donor cells; this fact may play a role in the function of EV molecule interactions.

Mutant KRAS plays a pathogenic role in many different types of cancer (Belda-Iniesta et al., 2008, Piva et al., 2014, Zhu et al., 2021) and has been shown to be present in EVs of tumour cells (Demory Beckler et al., 2013). Based on its known oncogenic function and ability to form complexes (Jaeger et al., 2022, Waninger et al., 2022, Zheng et al., 2022), we hypothesised that EV-KRAS could represent an important mediator of tumour-driven inflammation/tumour progression, and a potential candidate for a 'group leader' that can form complexes with other EV derived proteins to generate new biological effects. We took advantage of a proximity-based labelling system, BioID (a biotin ligase mutated), to promiscuously biotinylate proteins that interact with KRAS and are within 10–30 nm (Kim et al., 2014, Roux et al., 2012, Sears et al., 2019) as a means to identify the hypothesised EV-KRAS network. In contrast to many other affinity capture approaches for studying protein–protein interactions, BioID does not rely on physical protein–protein binding within native cell lysates. This feature allows the identification of protein proximities of weak or transient and dynamic natures. We identify new targets for EV-KRAS-driven lung inflammation, allowing identification of KRAS associated proteins vital for oncogene function. We demonstrate how KRAS serving as a leader molecule works with other molecules to promote induction of inflammation via EV-Fn1 mediated induction of interleukin-17A (IL-17A) in EV recipient cells. This approach revealed that the EV-KRAS/Fn1 centered complex network drove the expression of IL-17A, which in turn induced an array of downstream inflammatory cytokines in lung.

2 | RESULTS

2.1 | The composition of EV derived G12D-mutant KRAS protein complex is different from intracellular KRAS protein complex

The majority of the data published on KRAS protein indicate that it is an early player in many signal transduction pathways (Takács et al., 2020). KRAS is tethered to cell membranes, leading to the recruitment of numerous factors, subsequently forming KRAS complex which is a crucial step in the process of KRAS-mediated cell proliferation and differentiation.

Recently published data indicated that KRAS can also be sorted into EVs (Demory Beckler et al., 2013). Whether the KRAS complex in EVs has the same composition as in the EV producing cells is unknown.

The KRAS proto-oncogene is the most frequently mutated oncogene in cancer. Glycine-12 mutations are the most common substitution in cancer (Muñoz-Maldonado et al., 2019). For this reason, KRAS(G12D) was used throughout this study. To examine the network of proteins that interact with KRAS, we adapted the promiscuous biotin ligase (BirA*) approach. We employed a biotin ligase-tagging approach, in which tagged KRAS proteins biotinylate neighbour proteins in a proximity-dependent fashion, and proteins that interact with KRAS are identified via mass spectrometry (MS) sequencing. First, we generated recombinant lentivirus that expresses HA-birA*-KRAS(G12D). HEK 293 cells were transfected with 5 μg mutant-G12D (pLEX-HA-birA*-KRAS(G12D)-IRES-Puro; Addgene: 120562). G12D-mutant KRAS lentivirus was generated (Figure S1) in 293 cells using the lipofectamine transfection method. Supernatant containing viral particles were collected at 48 and 72 h following transfection. Concurrently, LL1 and TC1 lung epithelial cells were seeded in six-well cell culture plates and transduced with G12D-mutant KRAS lentivirus in the presence of polybrene (5 mg/ml) for 24 h. The respective cells were selected in the present of puromycin (2 mg/ml) for 72 h after initial transfection, then eGFP positive cells were FACS sorted (Figure S2a). To isolate their EVs, the selected cells were cultured in EV-free complete media (DMEM, 10% EV-free FBS and penicillin-streptomycin cocktail) and upon 70–80% confluency the cells were treated with biotin (50 mM) for 24 h before the supernatants were collected for isolation of EVs and cells were lysed as per the BioID protocol (Roux et al., 2013). The EVs released from cells were isolated by differential centrifugation (Lobb et al., 2015). The collected EVs were further purified using sucrose density gradient centrifugation (Figure S2b) and confirmed by the presence of eGFP using confocal microscopy (Figure S2c). The size, and concentration of EVs was calculated using a Nanosight (Figure S2d). The ultra-structure and morphology were confirmed by electron microscopy (Figure S2e). The EVs were validated with EV markers including CD63, CD81 and CD9 which were present in the EVs and calnexin, a non-EV protein was absent in the EVs (Figure S2f). Nanosight analyses show that CD9, CD63 and CD81 markers are positive on
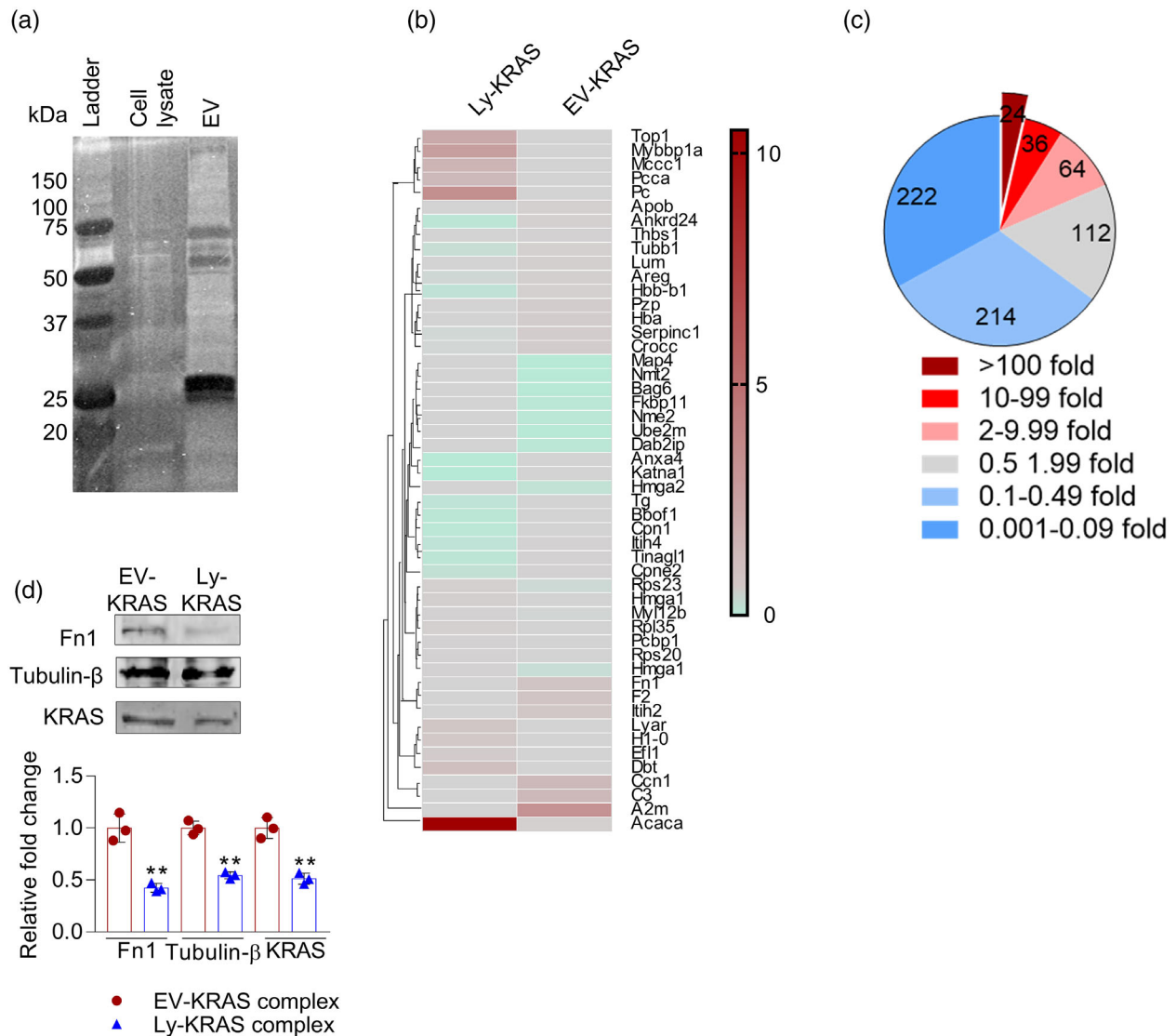
FIGURE 1 Proteins interacting with extracellular vesicular (EV) G12D-mutant KRAS are different from those that interact with intracellular G12D-mutant KRAS. (a) A representative image shows silver stained proteins from EV and cell lysates pulled down with streptavidin after running PAGE. (b) Heat map of proteins highly abundant or absent in EV-KRAS complex (EV-KRAS) group compared to the cell lysate-KRAS complex (Ly-KRAS) group, scale represents fold change in absolute abundance. (c) Pie-chart showing the number of proteins in the EV-KRAS subset analyzed by mass spectrometry (MS). (d) To confirm mass spectrometry data, western blots for Fn1, tubulin-β and KRAS were performed showing the differences in streptavidin pull down proteins from EV and cell lysates. Data are from three replicates.

the EVs (Figure S2g,h). The purity of sucrose gradient purified EVs was further evaluated by analysis of the number of EVs/mg of protein (Figure S2i).

To identify proximal protein interactions with KRAS inside of the cell and EVs, the proteins from whole cell lysates and EVs were pulled down using streptavidin bead technology and pulled down proteins were run on PAGE and silver stained. The patterns of silver-stained proteins from whole cell lysates and EVs were different (Figure 1a), suggesting that the proteins interacting with KRAS inside the cell are different from the proteins in the EVs. To identify KRAS proximal interacting proteins, streptavidin pulldown KRAS complexes were further analysed by mass spectrometry (MS), which demonstrated the presence of a different set of proteins in EV derived-KRAS complex (EV-KRAS) when compared to whole cell lysate-KRAS complex (Ly-KRAS) (Figure 1b, Table S1).

Comparison of the relative levels for each protein in the Ly-KRAS versus EV-KRAS revealed unique patterns of protein secretion and retention. For example, 24 proteins including Fn1 were highly enriched in EV-KRAS compared with the Ly-KRAS, whereas other proteins showed selective enrichment in the Ly-KRAS, and still other proteins were rarely found or not at all in EV-KRAS despite being present in Ly-KRAS (Figure 1c, Table S1). We also noticed that some proteins, such as Rho-associated protein kinase 2, phosphoglycerate mutase 1, peroxiredoxin-2 and EH domain-containing protein 1, showed nearly the same

levels in EVs and cell lysates (Table S2). Thus, these proteins could be used as reference proteins to demonstrate that similar levels of EV-KRAS and Ly-KRAS are used. The MS data were further verified using western blot analysis of Fn1 and tubulin-β in EV and whole cell protein lysate, which showed EV-KRAS had higher amounts Fn1 and tubulin-β (Figure 1d).

2.2 | Extracellular vesicular G12D-mutant KRAS protein complex induces more severe lung inflammation than intracellular KRAS protein complex in a mouse model

To determine whether the phenotypic effect of EV-KRAS on EV recipient cells is different from Ly-KRAS, TC1 EV-KRAS and Ly-KRAS were encapsulated in liposomes (isolated from mulberry bark EV-like particles [Sriwastva et al., 2022]) using a bath sonication procedure (Kumar et al., 2021). Mulberry bark derived extracellular vesicle lipid containing large numbers and variety of lipids are selectively used for packing K-RAS complex for the following reasons. Mulberry bark EV-like particle derived lipids have high efficiency for packing protein (Sriwastva et al., 2022). Additionally plant lipids play an essential role in plant tolerance to cold, heat and drought (Bhusal et al., 2021, Moreau et al., 1998, Niu & Xiang, 2018, Schwanz & Polle, 2001, Zhang et al., 2019) which are the major factors contributing to the instability of liposomes. Plants have developed strategies against cold, heat and drought and utilise an optimised lipid profile that enhances the plants survival and growth over many decades. Therefore, we utilised the plant anti-cold-heat-drought feature to make liposomes. In this study, we used the liposomes made from total lipids extracted from mulberry bark EV-like particles for delivering KRAS protein complex. Mulberry bark EV-like particles were isolated from a single batch of mulberry tree bark using the method we published (Sriwastva et al., 2022). The quality of each lot of mulberry lipid derived liposomes was determined by measuring the proliferation of TC1 cells transfected with liposomes listed in the figure (Figure S3a). Additional measurements of the size, number, TEM analysis and zeta potential were made for liposomes and liposomes loaded with TC1 EV-KRAS (Liposome-EV-KRAS) (Figure S3b-d). To determine whether loaded proteins are located on the lipid membrane or inside the lipid layer, the liposome-EV-KRAS proteins were coated on latex beads (4 μm) and permeabilised/non-permeabilised, stained with anti-mouse Fn1 antibody followed by FITC labeled secondary antibody and analyzed by flow cytometry. The results indicate that the permeabilization of EV leads to increasing Fn1 positive liposomes compared to unpermeabilised samples (Figure S3e), suggesting that the majority of Fn1 associated with EV-KRAS is located inside the liposomes. To further determine whether EV-KRAS associated proteins are protected by liposomes, liposome-EV-KRAS was digested for 1 h with proteinase K or PBS as a control; the digested liposome-EV-KRAS were centrifuged. The amount of liposome protein in the supernatant was analysed. The results indicated that protein concentration was unaffected as a result from proteinase K digestion (Figure S3f).

Next, the biological effect(s) of generated liposomes were evaluated. For potential future clinical utility of the results generated from this study, the human cell line H1299 was used as well for evaluating the effect of liposome-EV-KRAS and liposome-Ly-KRAS on the proliferation of human H1299, and murine LLC-1 and TC1 cells since the human KRAS protein has 96% homology with mouse KRAS (Figure S3g) and KRAS is one of the major players in driving cell proliferation. Empty liposomes were used as a control in addition to PBS. In vitro proliferation assessment showed that H1299, LLC-1 and TC1 cells treated with liposome-EV-KRAS had significantly higher proliferation rates compared to liposome-Ly-KRAS, empty liposomes and PBS controls (Figure 2a). The in vitro proliferation data prompted us to further investigate whether TC1 EV-KRAS had a different phenotypic effect from Ly-KRAS in mice when administered intratracheally (Figure 2b). Mice treated with liposome-EV-KRAS showed higher levels of acute inflammation and a more robust infiltration of immune cells in lung tissue as demonstrated by HE lung tissue staining (Figure 2c). Cytokine array data generated from mouse lung tissue lysates showed that proinflammatory cytokines and other inflammatory proteins, that is, IL-6, TNFα, IL-17A, MMP9, TIM-1, IGFBP-3, MMP-2 and FGF21 were significantly upregulated in liposome-EV-KRAS treated mice compared with liposome-Ly-KRAS treated mice (Figure 2d). The cytokine array data were further confirmed by ELISA for IL-6, IL-17A, FGF21 and TNFα (Figure 2e), and validated by gene expression analysis (mRNA quantification) (Figure S3h) as well as immune-confocal microscopy (Figure 2f).

To determine whether the in vitro and in vivo data generated from liposome-EV-KRAS have similar phenotypes as TC1-KRAS-G12D mutant-EVs, TC1 cells and mice were treated with liposome-EV-KRAS, TC1-KRAS-G12D mutant-EVs and PBS and liposome as controls. The outcomes demonstrated that liposome-EV-KRAS promotes TC1 cell proliferation (Figure S3i) and causes overproduction of lung IL-6, TNF-α and IL-17A (Figure S3j) at similar levels as TC1-KRAS-G12D mutant-EVs (EVs).

Additionally, we performed FACS analysis of lung cells and tissue to demonstrate that cells were taking up PKH26 positive liposome-EV-KRAS. Results showed that within CD11b, CD11C, CD3 gated regions, lung macrophages (F4/80) and T cells (CD3$^+$CD8$^+$) but not NKT cells (NK1.1$^+$CD3$^+$) take up PKH26 labelled liposome-EV-KRAS (Figure S4a). Taking up liposome-EV-KRAS led to much higher KRAS expression in PKH26$^+$ lung cells (67.0%) (Figure S4b) compared with KRAS (0.01%) expressed in the lung cells of mice treated with free PKH26 dye.
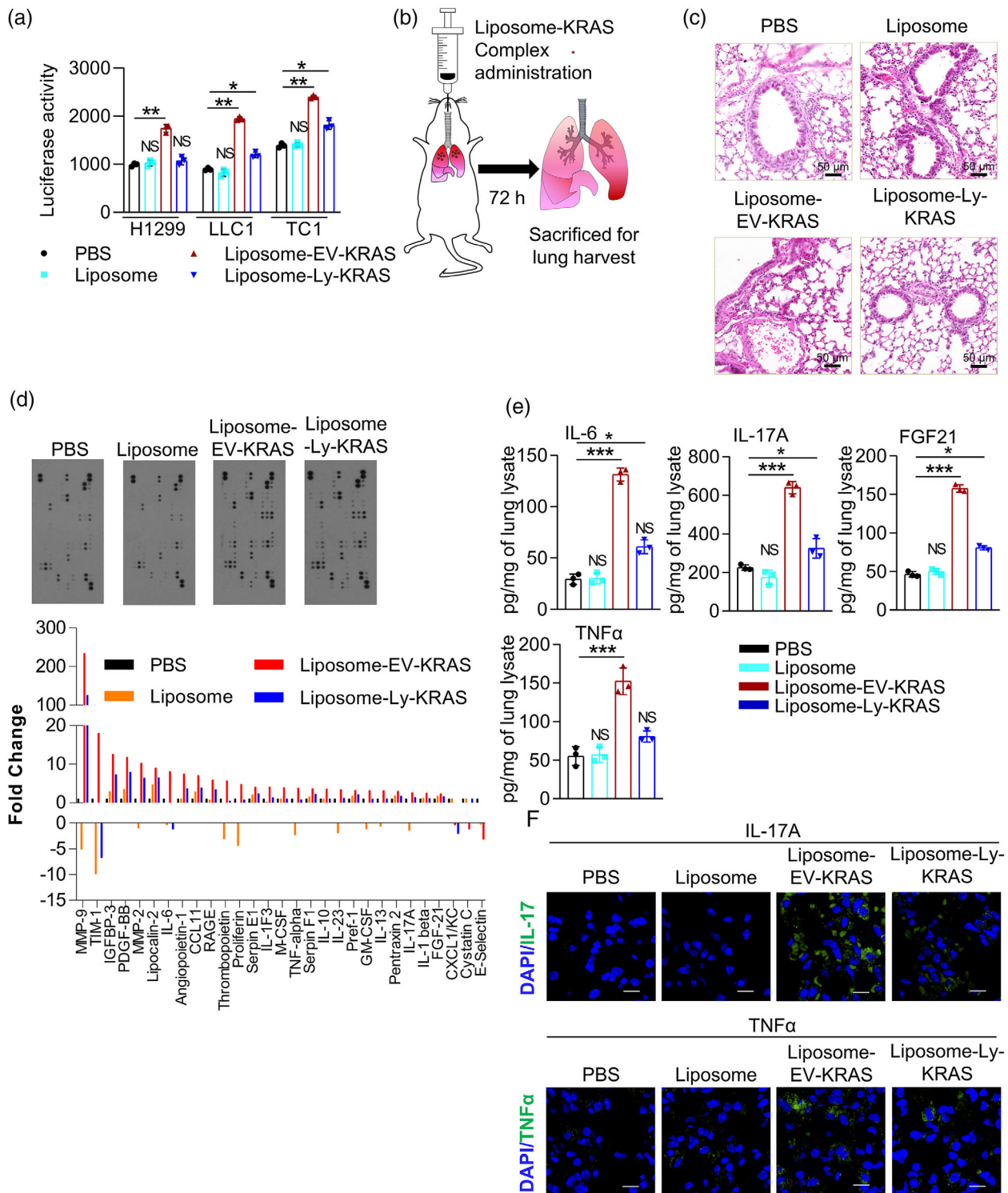
FIGURE 2 Effect of KRAS proximal proteins on tumour cell proliferation, lung inflammation, cytokine production and immune cell activity in B6 mice: (a) Effect of mutant KRAS extracellular vesicle (EV) complex on the proliferation of H1299, LLC1 and TC1 cells. (b) Schematic diagram showing intratracheal administration of KRAS complex. (c) Haematoxylin and eosin (HE) staining of lung tissue treated with KRAS complex from EVs and cell lysate (Ly) loaded in liposome (liposome-EV-KRAS/ liposome-Ly-KRAS). (d) Comparison of cytokine expression in lung tissue harvested from mice treated with PBS, liposome, liposome-EV-KRAS and liposome-Ly-KRAS, fold change represent pixel density. (e) ELISA for IL-6, IL-17A, TNFα, and FGF21 from lung tissue lysate showing T cell response to KRAS complex loaded in liposome following intratracheal administration. (f) Confocal microscopy for IL-17A and TNFα positive cells in lung tissue (scale: 10 μm). Mice were administered with 50 μl of 10×10^{10} liposome particles/ml. Data are mean ± SEM from five replicates, **$p < 0.01$ using one-way ANOVA.

2.3 | EV G12D-mutant KRAS complex induces lung inflammation via Fn1 mediated induction of IL-17A

The STRING (https://string-db.org, Search Tool for the Retrieval of Interacting Genes/Proteins) database aims to integrate all known and predicted associations between proteins, including both physical interactions as well as functional associations. Based on MS/MS data from EV-KRAS and Ly-KRAS, we next performed STRING database pathway analysis. The results suggested that Fn1, which was highly enriched in EV-KRAS, did not appear to directly interact with KRAS (Figure S5), but is a molecule that interacts with a group of proteins present in the EV-KRAS (Figure 3a). We then determined whether EV-KRAS-associated Fn1 plays a role in the induction of inflammatory cytokines by the EV-KRAS. The STRING database pathway analysis indicated that Fn1 not only interacts with a cluster of inflammatory cytokines (Figure 3b,c), but also regulates the expression of three additional clusters of related genes that promote tumour growth and IL-17A induction (Figure 3c). Next, to experimentally test whether EV-KRAS derived Fn1 plays a causative role in the induction of these cytokines, Fn1 was depleted from the EV-KRAS (EV-KRAS-Fn1-D) with anti-Fn1 antibody and the eluted proteins from Fn1-depleted EV-KRAS were again encapsulated in a lipid bilayer and administered to mice intratracheally. Mice that were administered liposome-EV-KRAS-Fn1-D showed a reduced inflammatory response in comparison to those that received Fn1-sufficient liposome-EV-KRAS as demonstrated by reduced inflammatory tissue damage (Figure 3d) and decreased levels of IL -17A, TNFα and IL-6 (Figure 3e).

IL-17A has been reported as a master regulator of proinflammatory cytokines (Xu & Cao, 2010). Using the same protocol described in Figure 2b, we employed wild-type and IL-17 receptor knockout (IL-17R KO) mice (C57BL/6J background) to test whether IL-17A is involved in EV-KRAS mediated lung inflammation. The IL-17R KO mice treated with liposome-EV-KRAS had a reduced level of acute inflammation and lower infiltration of immune cells in lung tissue as demonstrated by HE tissues staining (Figure 3f). ELISA data generated from mouse lung tissue lysate showed that IL-17R KO leads to a reduction of IL-6 and FGF21 (Figure 3g).

The potency of EV-KRAS in terms of induction of IL-17A expression compared with TC1- EVs was further evaluated. Mice administered intratracheally with liposome-EV-KRAS have no difference in induction of expression of IL-17A compared to TC1-EVs treatment and the expression of IL-17A is diminished in Fn1 depleted in the liposome-EV-KRAS group (Figure S6a).

To determine whether Fn1 is upstream of the molecule that promotes the expression of IL-17A, Jurkat cells were transfected with IL-17A-luciferase reporter gene for 24 h before being treated with liposome-EV-KRAS, liposome-EV-KRAS-Fn1-D or liposome-EV-KRAS-Fn1-D with exogenous recombinant Fn1 (liposome-EV-KRAS-Fn1-D + Fn1). The luciferase assay results revealed that IL-17A promoter activity was increased in liposome-EV-KRAS, whereas depletion of Fn1 from EV-KRAS led to a reduction of IL-17A promoter activity, and a reduction of TNFα and IL-6 induction. In contrast, addition of exogenous Fn1 to the liposome-EV-KRAS-Fn1-D group restored IL-17A promoter activity as well as TNFα and IL-6 induction. (Figure 3h).

To determine whether liposome-EV-KRAS has an increased or enhanced ability to induce expression of IL-17A in lung epithelial cells, we treated TC1 cells with liposome-EV-KRAS, liposome-Ly-KRAS and liposome and PBS as controls. qRT-PCR results indicated that the liposome-EV-KRAS has a higher ability to induce IL-17A expression than liposome-Ly-KRAS (Figure S6b). We then measured the level of KRAS and Fn1 in liposome-EV-KRAS and liposome-Ly-KRAS since they have distinct phenotypes. The results showed that liposome-EV-KRAS has higher levels of KRAS and Fn1 than liposome-Ly-KRAS although it was not statistically significant (Figure S6c). Collectively, our data support a conclusion that Fn1 contributes to EV-KRAS mediated lung inflammation through activation of the IL-17A/IL-17R signalling pathway in liposome-EV-KRAS recipient cells including both T cells and lung epithelial cells.

2.4 | EV G12D-mutant KRAS protein complex promotes lung tumour growth

IL-17A works by broad mechanisms to promote tumour progression as noted by: (1) the IL-17A mediated recruitment of immunosuppressive myeloid cells including CD11b^{+}Gr-1^{+} cells in a chemokine dependent manner, which can hinder effector cytotoxic T-cells or make the tumour microenvironment more 'angiogenesis-friendly', and acts as a mitogenic stimulant (Kuen et al., 2020); and (2) cancer intrinsic IL-17A signalling that leads to enhanced cancer cell survival/proliferation, epithelial–mesenchymal transition (EMT) and activation of the NOTCH and WNT signalling pathways (Wang et al., 2014, Wang et al., 2018, Wu et al., 2016).

To determine whether EV-KRAS contributes to induction of these pathogenic effects as reported in the literature (Demory Beckler et al., 2013, Muñoz-Maldonado et al., 2019) and described above, we used a mouse lung tumour model. First, to confirm that liposome containing KRAS complexes were taken up by TC1 cells, we labelled liposomes containing KRAS complex using PKH26 dye with a published protocol (Teng et al., 2018). TC1 cells were cultured for 6 h in the presence of PKH26 labelled liposome-EV-KRAS (2×10^8 nanoparticles/ml) in 1 ml serum-free culture medium with/without four uptake inhibitors (bafilomycin, 100 nM; amiloride, 100 M; chlorpamazine, 10 g/ml; and cytochalasin D, 1 g/ml) or an equal amount of free PKH26 dye as detected on the PKH26 labelled liposome-EV-KRAS as a control. After 6 h the cells were washed three times with PBS, fixed and analysed by flow cytometry. Results demonstrated that 77.4% of TC1 cells took up liposomes only, 79.5% of the TC1
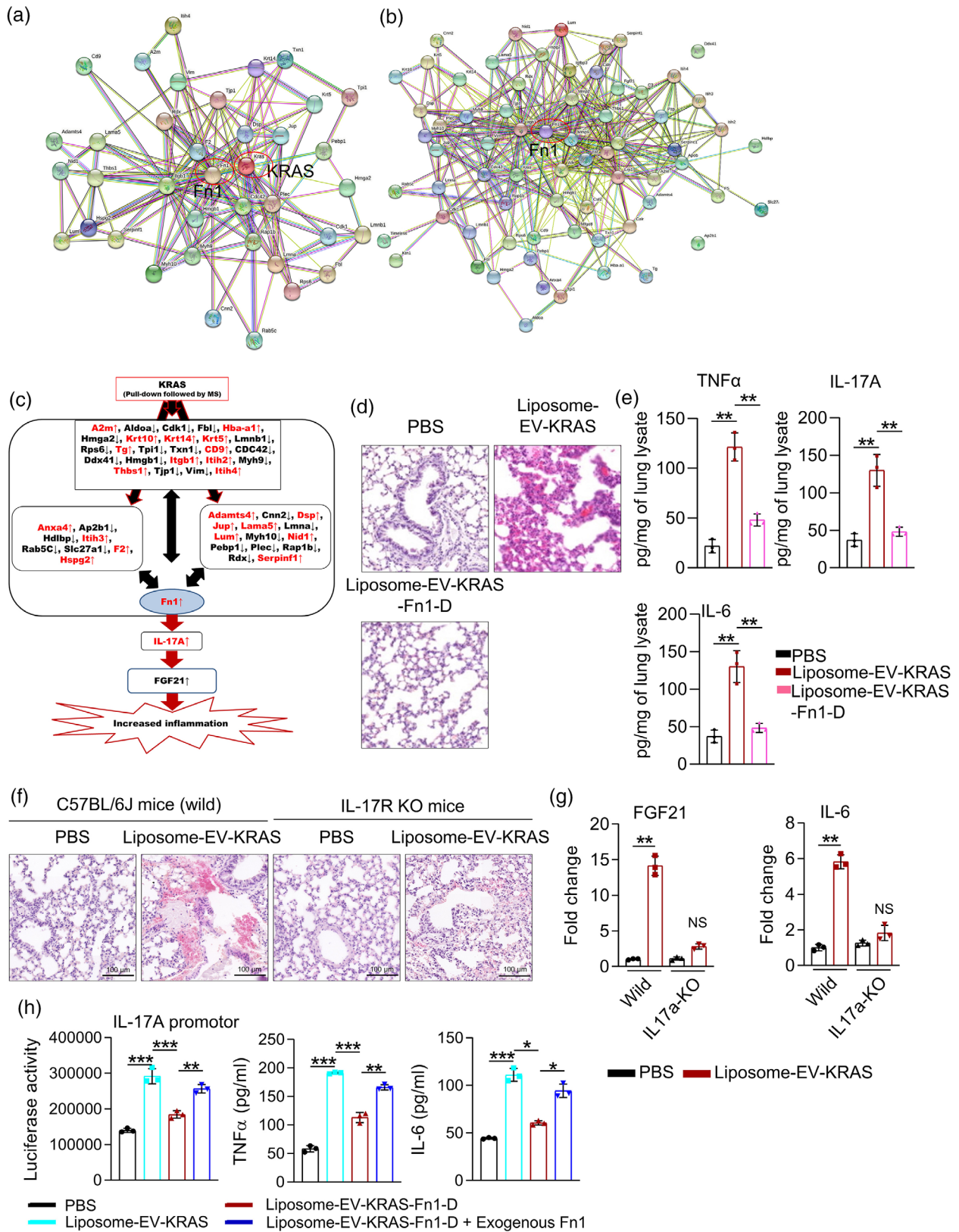
FIGURE 3 Fn1 plays a central role in extracellular vesicle (EVs) KRAS mediated inflammation in vivo: (a) Enrichment analysis based on MS analysis using the STRING database. (b) Enrichment analysis by the STRING database using proteins that were abundant in the EV KRAS complex (EV-KRAS) based on MS analysis and the cytokines upregulated following EV-KRAS intratracheal administration. (c) Pathway analysis showing KRAS mediated inflammation. (d) HE staining of lung tissue from the mice, intratracheal administered with PBS, liposome-EV-KRAS and Fn1 depleted EV-KRAS complex (liposome-EV-KRAS-Fn1-D). (e) ELISA for lung tissue TNFα, IL-17A and IL-6 from mice after intratracheally being administered liposome-EV-KRAS-Fn1-D.

(Continues)

cells took up liposome-EV-KRAS and 78.6% of the TC1 cells took up liposome-Ly-KRAS (Figure 4a). PKH26-positive cells are greatly reduced when cells are treated with the inhibitors, amiloride, cytochalasin D, bafilomycin but not chlorpromazine inhibitor, suggesting that liposome-EV-KRAS is taken up via multiple pathways (Figure S7a). In conclusion, the FACS analysis results suggest that PKH26 positive cells are significantly decreased when the cells were treated with inhibitors bafilomycin and amiloride whereas less than 1% of PKH26 positive cell was observed when treated with free dye PKH26. This result demonstrated that our PKH26 labelled TC1-EVs are taken up by TC1 cells via a specific pathway.

We then determined whether repeat transfection of TC1 with liposomes can increase the transfection efficiency. The TC1 cells were treated with PBS, liposome only (vehicle control), liposome-EV-KRAS or liposome-Ly-KRAS for three consecutive days until the cell confluency reach 70%–80%. TC1 cells treated for three consecutive days had higher PKH26 +ve cells on day 3 compared to a single dose treatment of PKH26 labelled liposome-EV-KRAS (Figure S7b). The trypsin digested TC1 cells were washed and reconstituted in PBS and intratracheally administered as a single dose of 3×10^5 cells/mice. After 12 weeks, the lungs were harvested assessed for tumour burden (Figure 4b). The mice that were administered liposome-EV-KRAS treated TC1 cells had the highest percent of tumour burden and number in sectioned lungs (Figure 4c-e). KRAS gene expression in tumour tissue was highly increased in the liposome-EV-KRAS group (Figure S7c). CD11 and Gr-1 double-positive cells were also significantly higher in mice administered liposome-EV-KRAS treated TC1 cells compared to mice treated with liposome-Ly-KRAS (Figure 4f).

Flow cytometry analysis of immune cells from lung tumour tissue revealed that mice that received liposome-EV-KRAS had lower Granzyme B^{+ve} and IFNγ^{+ve} T-cells compared to control or liposome-Ly-KRAS (Figure 4g). Consistent with Figure 2 data, ELISA results demonstrated that the liposome-EV-KRAS group had higher expression of IL-17A, IL-6 and FGF21 (Figure 4h).

Gene expression analysis of transcription factor genes, including ETS1, Zeb1, Zeb2, Foxc2, Vimentin, Fibronectin, Cadherin, ZO-1, Desmoplakin (DSP), SNAI1, SNAI2, TGFβ and Twist-related protein 1 (TWIST1), that are involved in EMT and induction of cancer stem cells were highly upregulated in the liposome-EV-KRAS group. Gene expression analysis suggested that liposome-EV-KRAS regulated the expression of genes such as IL4, IL6, IL10, IL-17A, KRAS, TNFα, MMP9, CXCL9, FGF21 and ITGB1. Genes involved in the NOTCH and WNT signalling pathways that promote tumour growth were also highly upregulated (Figure 4i).

2.5 | EV-KRAS complex facilitates lung inflammation through IL-17A/FGF21 axis

Next, we utilised in vivo and in vitro models to determine whether lung inflammation induced by the EV-KRAS complex is mediated via the IL-17A/IL-17R pathway leading to induction of FGF21. In vivo, mice were intraperitoneally administered IL-17R/Fc and anti-FGF21 antibody to neutralise IL-17A and FGF21, respectively. Mice were then administered EV-KRAS (i-t) and the lungs were analysed for acute inflammation as well as FGF21 levels after 72 h. H&E tissue staining and ELISA for anti-inflammatory genes demonstrated that neutralising IL-17A or FGF21 effectively diminished the EV-KRAS mediated inflammatory effect (Figure 5a,b). Furthermore, mice treated with IL-17R/Fc led to reduction of lung FGF21 (Figure 5b), consistent with the notion that the IL-17A/IL-17R pathway regulated induction of FGF21 gene expression.

To confirm this result, an ex vivo experiment was carried out. Jurkat-T cells were treated with PBS, liposome only, liposome-EV-KRAS or liposome-Ly-KRAS with/without depletion of IL-17A. Proliferation analysis using the ATP light assay showed that the liposome-EV-KRAS-induced Jurkat cell proliferation and FGF21 promoter activity was abrogated in the absence of IL-17A (Figure 5c,d). To explore the effect of FGF21 on pathways that contribute to tumour progression in the lung, lung tumour lysates were depleted with anti-FGF21 and used to treat TC1 cells. Western blot analysis of PI3K, SIRT1 and NF-κB suggested that depletion of FGF21 led to the loss of liposome-EV-KRAS mediated induction of PI3K, SIRT1 and nuclear translocation of NF-κB, all of which play an important role in tumour progression (Figure 5e). Gene expression analysis further suggested that FGF21 depletion also resulted in a failure to upregulate tumour invasion factors including SNAI1 and TWIST1 (Figure 5f). Collectively, our results generated from these experiments support the notion that EV-G12D-mutant KRAS protein complex promotes lung inflammation and lung tumour growth via the IL-17A-FGF21 axis.

3 | DISCUSSION

Herein, we used a proximity-based labelling system, BioID (a biotin ligase mutated), to promiscuously biotinylate proteins that interact with KRAS within 10–30 nm. We discovered an EV KRAS-driven protein network and further identified a unique role
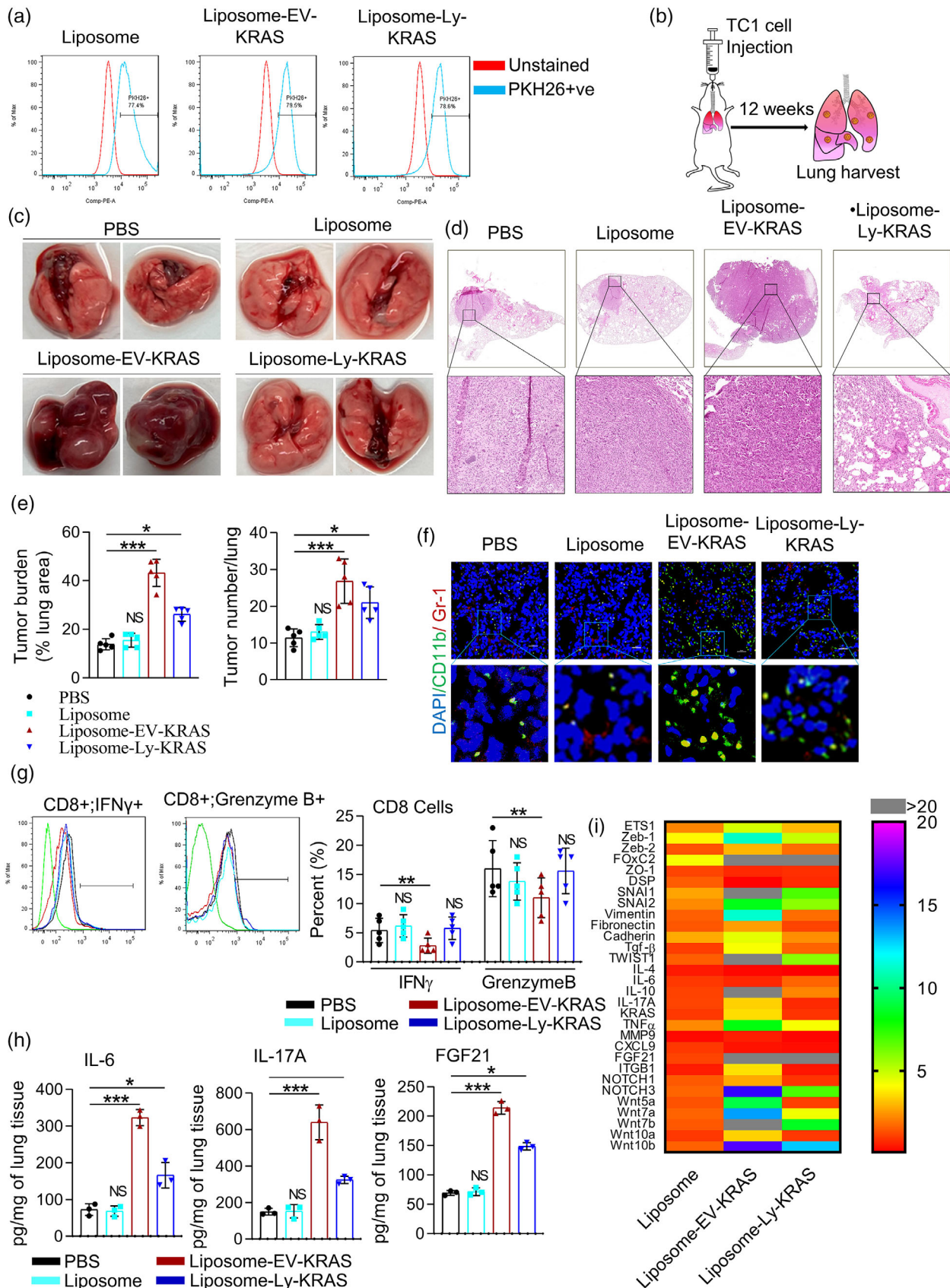
FIGURE 4 Extracellular vesicular (EV) KRAS complex is more potent in promoting lung tumour growth than KRAS complex from EVs donor cells: TC1 cells were treated for three consecutive days with liposome containing KRAS complex from EV or EV-donor cells (Cell lysate; Ly) and then administered

(Continues)

FIGURE 4 (Continued)

intratracheally to mice. (a) Uptake of liposome-EV-KRAS in TC1 cells. (b) Timeline of in vivo experiment for TC1 cell treatment for lung tumour development showing development of TC1 tumour following intratracheal administration of TC1 cells (PBS, liposome alone, liposome-EV-KRAS, or lysate KRAS complex (liposome-Ly-KRAS). (c) Pictorial representation of TC1 tumour development in mouse lung. (d) HE staining of TC1 tumours. (e) Tumour volume and number of nodules in lung tumours. (f) Immunostaining of CD11b and Gr-1 positive cells in lung tissue (scale: 20 μm). (g) Flow cytometry analysis of CD8 positive IFNγ and Granzyme B cells. (h) ELISA for IL-17A, IL-6 and FGF21. (i) Heat map showing expression of genes associated with in epithelial–mesenchymal transition. For TC1 lung tumour development, the respective liposome-KRAS treated TC1 cells (2×105 cells in 50 μl) were administered using the IMIT instillation procedure. Data are mean $\pm$ SEM from five biological replicates, *$p < 0.05$, **$p < 0.01$ using one-way ANOVA.

of the EV-KRAS protein network based on the following results: (i) MS/MS protein analysis indicated that EV-KRAS is clearly distinct from Ly-KRAS in terms of composition and biological effects on inflammation and tumour growth; (ii) EV-KRAS serves as an EV protein network organiser that assembles an Fn1 centered protein complex that induces lung inflammation; and (iii) Fn1 mediated induction of IL-17A in the EV recipient cells, and subsequent induction of FGF21 with the participation of the IL-17A/IL-17R signalling pathway.

The biological effect of EV proteins on EV recipient cells has been mainly studied on an individual protein basis, where genes encoding for an individual protein are knocked out individually by genetic deletion. This type of approach is limited in its ability to delineate what an EV complex contributes to the EV-driven biological effects on the recipient cells. By contrast, we show here for the first time that EV-KRAS triggers the activation of the IL-17A-mediated inflammatory pathway via the pre-formed KRAS/Fn1 complex in the EV-recipient cells.

A hallmark of cancer, including lung cancer, is an intense inflammatory reaction. In this report, we provide compelling evidence that IL-17A lies downstream of Fn1. Both Fn1 (Bazan-Socha et al., 2018, Hamsten et al., 2016, Wang et al., 2017, Zhou et al., 2022) and IL-17A (Akbay et al., 2017, Cai et al., 2019, Hagner et al., 2021, Salazar et al., 2020) have been shown to promote inflammation and tumour progression. Interaction of IL-17A with its receptor, which is expressed on a variety of cell types (including tumour cells and non-tumour cells), causes secretion of proinflammatory cytokines such as IL-6, various chemokines and factors that promote tumour progression. Whether EV-KRAS-Fn1 mediated induction of IL-17A plays a causative role in promoting tumour progression, on the other hand, will require further investigation.

One caveat of our study is that we have yet to determine which factor(s) cause the increasing size and charges of liposome-EV-KRAS when compared with liposomes alone. The factor(s) could be from EV-KRAS complex derived or unidentified factors (Sani et al., 2022, Sheikholeslami et al., 2022) including aggregation (Dhiman et al., 2022). Future work is needed to identify the involved factor(s).

We also noticed that the expression of the *KRAS* gene is increased in tumour tissue in mice administered liposome-EV-KRAS. This increased *KRAS* gene expression could take place in other types of cells present in the lung. The expression of *KRAS* gene could be induced in other types of lung cells via soluble factors released from liposome-EV-KRAS recipient cells or other types of cells contacting with liposome-EV-KRAS recipient cells. Future work is also needed to identify which type of lung cells have increased expression of KRAS due to liposome-EV-KRAS treatment.

Finally, our mechanistic findings have implications that reach beyond the basic biology of EV protein networks. A more in-depth understanding of how EV protein complexes impact disease is likely to result in the development of novel therapeutic approaches that are designed to co-modulate beneficial and harmful effectors of such complexes to the advantage of the patient.

4 | MATERIALS AND METHODS

4.1 | Cell culture and transfection

TC1, LLC-1 and H1299 cells were cultured in Dulbecco's Modified Eagle Medium (DMEM) media supplemented with 10% FBS, 100 U/ml penicillin and 100 μg/ml streptomycin. TC1 cells were transfected with birA*-KRAS G12D using a transfection kit (Invitrogen, Waltham, MA; cat. No. L3000-015) as per the manufacturer's instructions and in the presence of 5 μg/ml puromycin. The KRAS G12D positive cells were FACS sorted based on GFP^{+ve} cells and confirmed by confocal microscopy. Jurkat cells were culture in RPMI 1640 with 2 mM L-glutamine media supplemented with 10% FBS, 100 U/ml penicillin and 100 μg/ml streptomycin.

4.2 | Luciferase assay for FGF21 and IL-17 promoter activity in Jurkat cells

Dr. Wenke Feng (the University of Louisville, Louisville, USA) generously provided the mouse FGF21 reporter plasmids, which have promoter constructs 1497/+5 inserted into pGL3 (Promega) using the KpnI and XhoI sites. The lipofectamine 3000 transfection kit (Invitrogen, USA) was used to transfect cells with 2 g of the pGL3 promoter FGF21 (1497/+5).
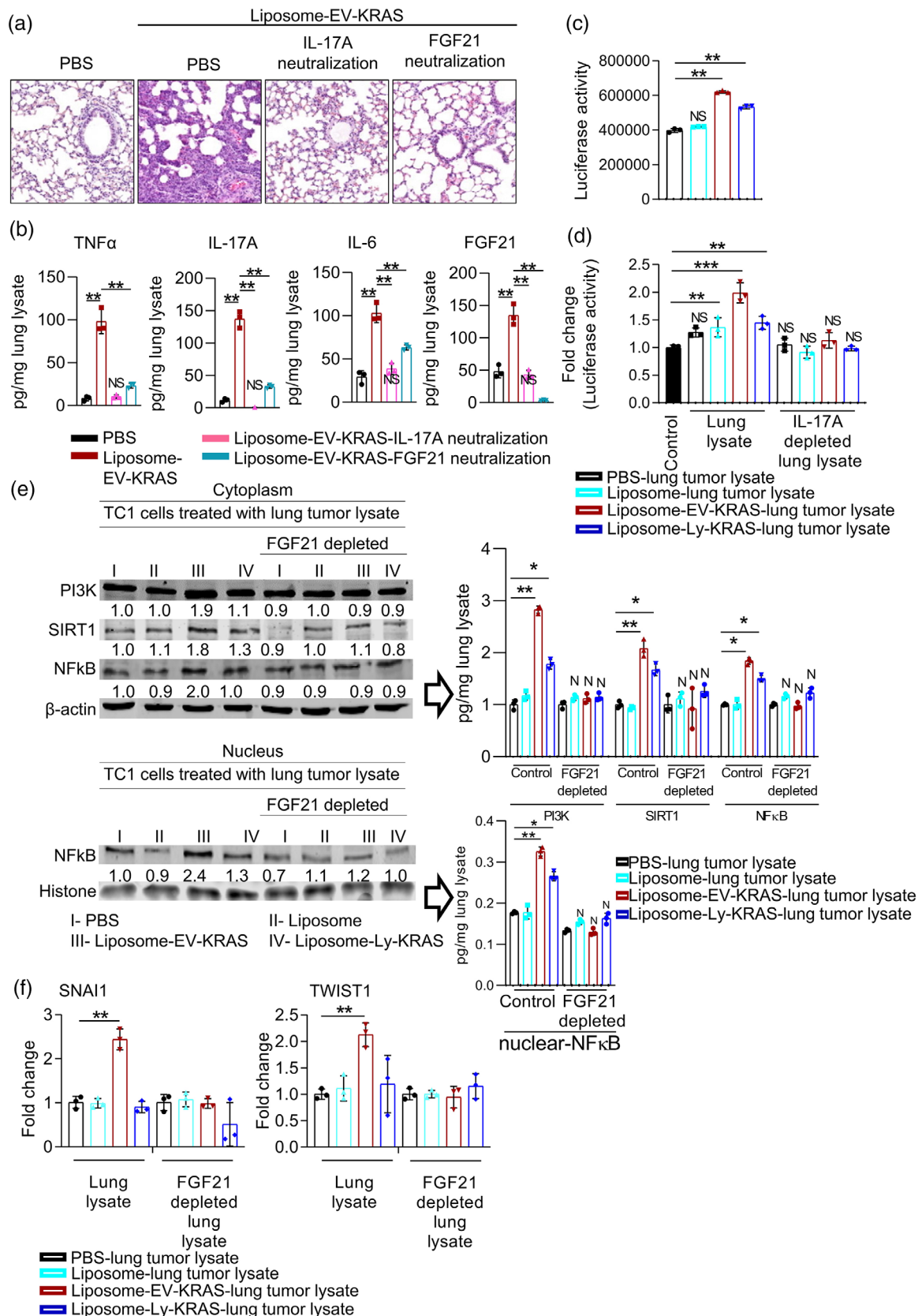
FIGURE 5 EV-KRAS complex facilitates inflammation through the IL-17A/FGF21 axis. (a) HE staining of lung tissue from mice (blocked with IL-17R/Fc or anti-FGF21 antibody) intratracheally administered extracellular vesicle (EV) KRAS complex (liposome-EV-KRAS). (b) ELISA for TNFα, IL-17A and IL-6 from lung tissue from mice (blocked with IL-17R/Fc or anti-FGF21 antibody) intratracheal administered liposome-EV-KRAS. (c) Adenosine triphosphate (ATP) cell proliferation assay showing proliferation of Jurkat cells in response to lung tumour lysate with and without IL-17A depletion using IL-17A

(Continues)

Jurkat cells were grown to 70% confluency and transfected with the luciferase reporter gene assay reagents obtained from Promega as per the manufacturer's instructions. Briefly, Jurkat T cells were co-transfected with a pGL3 luciferase reporter plasmid (Promega, Madison, WI) containing the proximal human IL-17F promoter region and a Renilla luciferase plasmid (pRL-CMV; Promega), as well as either an empty pcDNA3.1 plasmid. Cells were treated after 24 h of transfection as per the protocol and lysed 48 h after transfection. By co-transfecting 1 g of the GFP vector, the transfection efficiency was standardised. Luciferase activity was measured using a Dual-Luciferase Reporter Assay (Promega, Madison, WI) as per the manufacturer's instructions.

4.3 │ Preparation of lentivirus

A lentivirus preparation was made using a previously described method (Kumar et al., 2021). A lentivirus containing birA*-KRAS G12D (KRAS G12D) fusion protein was procured from Addgene (120562). TC1, LLC1, H1299 and 293T human embryonic kidney 293 cells (ATCC) were grown in Dulbecco's Modified Eagle's Medium (D-MEM; Gibco, Waltham, MA) maintained in presence of 10% fetal bovine serum (FBS), 2 mM l-glutamine, 100 U/ml penicillin and 100 μg/ml streptomycin (Gibco, Waltham, MA). The plasmid was transfected into 293T cells with a lentivirus using the Lipofectamine 3000 transfection kit (Invitrogen, USA). After 72 h of transfection, pseudovirus-containing culture media was collected, and the viral titer was calculated. GFP-TC1/LLC-1/H1299 cells were created using a lentivirus encoding birA*-KRAS G12D (KRAS G12D). TC1/LLC-1/H1299 (2×10^5) cells were plated into a six-well plate along with an appropriate amount of viral stock in the medium. After selection with puromycin, the cells with the highest expression of GFP were sorted using a BD FACSAria III cell sorter (BD Biosciences, San Jose, CA) and used for further downstream experiments. GFP expression was further confirmed by confocal fluorescence microscopy (Nikon, Melville, NY).

4.4 │ Isolation of EVs and analysis

The EVs from TC1 cells were isolated using a previously described method (Sriwastva et al., 2022). The TC1 cells were seeded at 30%–40% confluency in D-MEM medium in 100 mm cell culture flask supplemented with 10% EV-free FBS media and 5 μg/ml puromycin for 72 h. The media were collected and secreted EVs were collected using differential centrifugation. Briefly collected culture media was centrifuged at $4000 \times g$ for 30 min, the supernatant collected and centrifuged at $10,000 \times g$ for 1 h and the supernatant retained and preserved. The supernatant was further centrifuged at $100,000 \times g$ for 2 h at 4°C, the pellets collected and purified on a sucrose gradient (8%, 30%, 45% and 60% sucrose in 20 mM HEPES, 20 mM Tris-Cl [pH 7.2]). The protein concentration of purified EVs was determined using a BioRad Protein Quantitation Assay kit with bovine serum albumin as the standard. The purified EVs were analysed for size distribution and concentration using a NanoSight NS300 (Malvern Panalytical, Westborough, MA) at a flow rate of 30 μl/min.

The purified EV morphology was examined using electron microscopy. Purified EVs were fixed in 2% paraformaldehyde and imaged under a Zeiss EM 900 electron microscope using a previously described method (Mu et al., 2014).

The purified EVs isolated from the cells were stored in aliquots at –80°C until further downstream studies to avoid freeze-thawing effects.

4.5 │ Biotin tagged protein isolation and analysis

Biotin tagged proteins (KRAS complex) were isolated from whole cell and EVs using streptavidin pull down. Briefly, cells and isolated EVs were lysed on ice for 30 min using lysis buffer (0.5% Tween 20, 150 mM NaCl, 50 HEPES supplemented with protease inhibitor (cOmplete™ Protease Inhibitor Cocktail, Roche)) followed by centrifugation at $12,000 \times g$ for 20 min and the supernatant collected for downstream processing. An equal amount (2.5 mg) of total protein lysate from whole cell (TC1-G12D) lysate and TC1-EVs derived protein lysate was incubated with streptavidin magnetic beads for 1 h at 4°C. Biotin bound magnetic beads were washed thrice with lysis buffer to remove unbound protein. Proteins were eluted with elution buffer (4 mg/ml biotin,

25-mM Tris-HCl and 0.3-M NaCl; pH 8.5) and eluted proteins were visualised using silver staining of a PAGE gel, western blot and mass spectrometry (MS). The eluted proteins were stored in aliquots at $-80°$C until used in further downstream experiments.

The KRAS complex and EV biological activity (TC-1 proliferation quantified with the method as described in Figure S3i) was measured before storing at $-80°$C. Before use, each aliquot was thawed, and their biological activity (TC-1 proliferation) was measured again and the samples having no significant diminution of TC-1 proliferation activity compared to pre-freeze samples were used for the experiments conducted in this study.

4.6 | Liposome preparation

Liposomes were prepared using biotin tagged KRAS complex eluted proteins and total lipid isolated from mulberry bark derived EV-like nanoparticles (Sriwastva et al., 2022). Total lipids were extracted with chloroform and dried under vacuum. The nanoparticles were prepared as described earlier (Sriwastva et al., 2022). Briefly, 20 mg of lipid was suspended in 200–400 μl of 155 nM NaCl and the respective protein at a protein:lipid ratio of 0.1 followed by bath sonication (FS60 bath sonicator, Fisher Scientific) for 30 min. The KRAS complex encapsulated in a lipid bilayer (nanoparticles) was collected by centrifugation at $100,000 \times g$ for 1 h at 4°C and washed in PBS. Liposome with and without EV-KRAS suspended (liposome-EV-KRAS) in 1X phosphate buffer saline were analyzed for size and number using the Nanosight NS300 (Cambridge, UK), zeta potential was analyzed using a Zetaview (Cambridge, UK) and transmission electron microscopy was performed (Apreo C LoVac FESEM; Thermo-Fisher Scientific, MA). To confirm and validate the loaded KRAS complex proteins on liposomes western blot was done (Figure S6d).

The liposomes were labelled with PKH26 as per the manufacturer's instructions and $\sim 1 \times 10^{10}$ liposomes/ml were suspended in diluent C, stained with 2 μM PKH26 for 15 min at room temperature and washed three times with PBS by ultracentrifugation $100,000 \times g$ for 2 h at 4°C. The prepared liposomes were stored at $-80°$ for further downstream experiments. The PKH26 labelled liposomes were used immediately without any long-term storage, otherwise all working liposomes were kept on ice (Dehghani et al., 2020).

Total of 50 μl of each liposome-EV-KRAS fraction were incubated with 0.25 μl of aldehyde/sulfate-latex beads (ø = 4 μm; 5.5×10^6 particles/ml; Invitrogen, Carlsbad, CA) for 15 min at RT. Bead-coupled liposome-EV-KRAS EVs were centrifuged at $2000 \times g$ for 10 min to form pellets, which were then washed with PBS and centrifuged once more. For permeabilisation of liposome-EV-KRAS, the latex attached liposomes-EV-KRAS were permeabilised by fixation. The permeabilisation Buffer Set (eBioscience) was used to fix and permeabilise liposomes for intra-vesicular staining. After incubation, the samples were washed twice with 1 ml of permeabilisation buffer and then resuspended in 100 μl PBS with 0.5% bovine serum albumin. Anti-Fn1 antibody was used as the primary staining antibody for 1 h at room temperature (RT), followed by FITC-conjugated secondary antibodies for 30 min at RT. Latex beads alone and latex beads coupled to liposome-EV-KRAS without primary mAb served as negative controls. After secondary staining, 500 ml of PBS was used for two rounds of washing followed by a 10-min, $2000 \times g$ centrifugation at 4°C. A flow cytometer (FACSCanto A, BD Biosciences, San Jose, CA) was used to collect the data, which was then analysed using FlowJo software (version Tree Star, Ashland, OR).

To determine the purity of the liposome-EV-KRAS, the liposome-EV-KRAS was digested with proteinase K or PBS as a control for 1 h, and the digested liposome-EV-KRAS were then centrifuged to determine whether EV-KRAS associated proteins are protected by liposomes. Protein content in liposomes was measured using the BCA technique.

4.7 | Mice

Female C57BL/6 (wild and IL-17R knock out (KO)) mice (aged 8- 10 weeks) were purchased from the Jackson Laboratory (Bar Harbor, ME) and maintained on a 12-h/12-h light/dark cycle in a pathogen-free animal facility at the University of Louisville. Animal handling was performed following the Institute for Laboratory Animal Research (ILAR) protocol, and all animal experiments were conducted in accordance with protocols approved by the University of Louisville Institutional Animal Care and Use Committee (Louisville, KY).

4.8 | Lung specific intratracheal instillation for lung inflammation and tumour development

The administration of liposome, EV KRAS complex encapsulated in liposomes (liposome-EV-KRAS); cell lysate KRAS encapsulated in liposomes (liposome-Ly-KRAS)) or tumour cells (TC1) were performed directly into the mouse lungs to study lung inflammation and tumour development as per a previously described method (Au - Lawrenz et al., 2014). Intubation-mediated intratracheal (IMIT) instillation is a non-invasive approach that allows for >98% administration into the lungs with excellent spread throughout the lung. To demonstrate that intratracheal administration of TC1 cells were equally distributed into the lung, we intratracheally administer PKH-26 labelled liposome-EV-KRAS, and results suggest that IMIT allowed for equal

biodistribution (Figure S6e). For the lung inflammation model, mice were given PBS, empty liposome nanoparticles (10×10^{10} particles/ml), liposome-EV-KRAS (10×10^{10} particles/ml) and liposome-Ly-KRAS (10×10^{10} particles/ml) in 50 μl volumes. Peripheral blood for plasma/serum collection was obtained 72 h after intratracheal injection, and mice were humanely sacrificed for lung harvesting for later analysis.

For TC1 lung tumour development, the respective liposome-KRAS treated TC1 cells (2×10^5 cells in 50 μl) were administered using the IMIT instillation procedure. The mice were followed for 12 weeks for tumour development and then humanely sacrificed.

Based on the descriptions and suggestions provided by the Mouse Models of Human Cancers Consortium, tumours were identified and outlined (Nikitin et al., 2004). Each lung lobe was first sectioned at the surface and then serially taken every 300 μm, resulting in an analytical depth of about 1200 μm. HE stained slides were examined with an Aperio ScanScope. Using QuPath (Open-source software), the tumour area from histologic sections was quantified. The sum of segmentations of individual tumours from all five sections was used to calculate the pulmonary tumour burden per mouse. Results are expressed as the percentage of lung occupied by tumour ([area tumour/area lung] $\times$ 100).

4.9 | Cytokine production analysis

The effects of EV and cell lysate derived KRAS complex on cytokine production in lung tissue were evaluated. The lung tissue was processed according to the instructions included in the Cytokine Array Kit. A Proteome Profiler Mouse XL Cytokine Array Kit was used to assess cytokines according to the manufacturer's instructions (R&D Systems, ARY028). HLImage++ (Western Vision Software) based on spot intensity in the arrays.

4.10 | In vitro uptake of labelled liposome-EV-KRAS

To test uptake efficiency of KRAS complex containing liposomes with and without EV-KRAS in TC1, LLC-1 and H1299 cells, cells were cultured at 37°C for 6 h with PKH26 tagged liposome-EV-KRAS (2×10^8 particle/ml). Before being fixed with 2% paraformaldehyde, the cells were washed three times in PBS. Fixed cells were collected using a BD FACSCanto flow cytometer (BD Biosciences, San Jose, CA). The cells were then analysed using FlowJo software (TreeStar Inc., Ashland, OR).

4.11 | Western blot analysis

Tissues or cells were rinsed in ice-cold PBS and homogenised. The cells/EVs were lysed in radioimmunoprecipitation assay lysis buffer supplemented with protease inhibitor for 30 min at 4°C and vortexed at full speed for 15 s. The lysate was centrifuged at 12,000 $\times$ g for 15 min at 4°C. Using bovine serum albumin as the reference, the supernatant was collected, and the protein concentration was measured using the BioRad Protein Quantitation Assay kit. SDS sample buffer (4X) was used to dilute the samples, which were separated using 12% sodium dodecyl sulphate PAGE and then transferred to nitrocellulose membranes (Bio-Rad). Specific antibodies (1:1000 dilution; Table S3) were used to detect individual proteins. Using infrared fluorescence secondary antibodies on an Odyssey CLx Imager, the protein bands were analyzed (LiCor Inc., Lincoln, NE).

4.12 | Flow cytometry

Stained cells were fixed with 2% paraformaldehyde (PFA) and stained for 40 min at 4°C using fluorochrome-conjugated antibodies (Table S3). After three washes with PBS, cells were acquired using a BD FACSCanto flow cytometer (BD Biosciences, San Jose, CA) and analyzed using FlowJo software (Tree Star Inc., Ashland, OR).

4.13 | Confocal microscopy

For frozen sections, periodate-lysine-paraformaldehyde fixed tissues were dehydrated overnight at 4°C with 30% sucrose in PBS before embedding in optimal cutting temperature compound. Using a microtome, tissue was then sliced into ultrathin (5 μm) slices followed by blocking with 5% BSA in PBS. Primary antibodies (Table S3) (1:800) were added to the mix and incubated overnight at 4°C. Secondary antibodies conjugated to a fluorescent dye (Alexa-flour 488/ Alexa-flour 595) were added to the sections after washing three times (at 1:2000 dilution). The nuclei were stained with 4′,6-diamidino-2-phenylindole dihydrochloride (DAPI). Tissues and cells were visualised using a confocal laser scanning microscopy (Nikon, Melville, NY).

4.14 | Histological analysis

Tissues were fixed in buffered 10% formalin solution (SF93-20; Fisher Scientific, Fair Lawn, NJ) overnight at 4°C for haematoxylin and eosin (H&E) staining. Dehydration was achieved by immersing the tissue cassette for 40 min in a graded ethanol series of 70%, 80%, 95% and 100% ethanol. Tissues were fixed in paraffin and then sliced into ultrathin (5 μm) slices with a microtome. Tissue sections were deparaffinised in xylene (Fisher), rehydrated in increasing concentrations of ethanol in PBS, stained with H&E, and scanned with an Aperio ScanScope (IL, USA).

4.15 | Elisa

Enzyme-linked immunosorbent assay (ELISA) kit (eBiosciences) was used to quantify the following cytokines: IL-6, IL-17A, TNFα, FGF21, Fn1 and KRAS as per the manufacturer's instructions and described earlier (Teng et al. 2021). For liposome-EV-KRAS proteins, the pelleted liposome-EV-KRAS was suspended in 50 μl radioimmunoprecipitation assay (RIPA) buffer (25 mM Tris.HCl pH 7.6, 150 mM NaCl, 1% NP-40, 1% sodium deoxycholate and 0.1% SDS) and incubated at 4°C for 30 min and placed in an ice-cold sonication bath for 30 s.

4.16 | RNA extraction and qRT-PCR

Total RNA was extracted using a RNeasy Mini Kit from the cells and tissue according to the manufacturer's instructions (Qiagen, 74104). RNA (1000 ng) was reverse transcribed into cDNA using SuperScript III reverse transcriptase and oligo dT primers (Invitrogen). According to the manufacturer's instructions, cDNA samples were amplified in a CFX96 Realtime System (Bio-Rad) using SYBR Green Master Mix (Invitrogen) and specific primers to quantify genes of interest. The fold variations in mRNA expression between treatments and controls were calculated using the CT method. Results were expressed as a fold increase over control/baseline levels, with each sample's results being corrected for the amount of GAPDH mRNA that was detected in the same samples, which is set at a value of 1.

4.17 | Fn1 depletion from EV-KRAS complex and lung tissue lysate

Lung tissues were washed with ice-cold PBS, homogenised and lysed in RIPA lysis buffer (1 ml/100 mg tissue) supplemented with protease inhibitor on ice for 30 min. The lysate was centrifuge for 15 min at 4°C and the supernatant was collected. For Fn1 depletion, protein lysate from EV-KRAS complex and lung tissue lysate was mixed with 50 μl of protein G agarose suspension and incubated for 3 h at 4°C on a rocking platform. The mixed solution was centrifuged at 12,000 × g for 10 min and the supernatant collected. The supernatant was mixed with anti-Fn1 antibody (Table S3) and incubated for 1 h at 4°C followed by addition of protein G agarose pre-washed with RIPA buffer and incubated for 3 h at 4°C. The samples were centrifuged and washed with citrate-phosphate buffer, pH 5.0, three times and the supernatant discarded. Elution buffer (200 μl) was added to the pellet for 5 min and then centrifuged. The supernatant was collected and stored at –80°C for further downstream processing.

4.18 | In vivo neutralisation of cytokines

In vivo cytokine neutralization experiments involved administering mAbs against FGF21 (Abclonal, Woburn, MA) and recombinant Mouse IL-17RA/IL-17R Fc Chimera Protein (R&D System) intraperitoneally. Mice received 100 μg of antibody or 50 μg of recombinant Mouse IL-17RA/IL-17R Fc Chimera Protein intra-peritoneally one day prior and 6 h after liposome-EV-KRAS administration.

4.19 | Enrichment analysis

Enrichment analysis was based on 304 proteins which were differentially expressed ($p < 0.05$, and more than 5-fold change) between samples in the MS analysis. Significantly regulated proteins were subjected to GO analysis and protein network analyses (STRING) using the STRING database. Enrichment analysis was followed by pathway analysis which was based on differentially expressed protein in the MS analysis and differentially expressed cytokines following intratracheal administration of liposome/liposome-EV-KRAS.

4.20 | KRAS-Fn1 interaction

To prove whether KRAS physically interacts with Fn1, KRAS protein 20 μg (Sino Biological; cat: 12259-H07E) was incubated with purified Fn1 (20 μg) (Sino Biological; cat: 10314-H08H) for 2 h and 30 min in 400 μl equilibrium buffer (20 mM Tris–HCl, pH 7.5, 250 mM NaCl). The protein mixture (KRAS-Fn1) was combined with the anti-KRAS antibody (2 μg), which was then incubated for 4 h at 4°C with gentle agitation. Pre-washed 100 μl protein G was added to the slurry of KRAS antibody-protein mixture and again incubated at 4°C for 4 h with gentle agitation. After centrifugation, the supernatant was removed and washed three times with equilibrium buffer. Beads were heated in 50 μl of 2 × SDS loading buffer without DTT for 10 min at 50°C to elute the antibody-protein complex, which was then separated on SDS PAGE and analysed by immunoblotting KRAS and Fn1.

We also analysed whether KRAS interacts with intracellular FN-1. TC1 cell whole cell protein was pulldown using KRAS antibody and followed by western blot analysis of Fn1.

4.21 | Statistical analysis

The data from three independent experiments were presented as mean ± SEM, and GraphPad Prism 7 was used for all statistical analysis. The means of two groups were compared using a t-test, and in experiments with more than two groups' data were analysed using the one-way analysis of variance test. Statistically significant significance is shown as $p \leq 0.05^*$, $p \leq 0.01^{**}$ and $p < 0.001^{***}$.

CONFLICT OF INTEREST
The authors declare no competing interests.

ORCID
Joshua L. Hood https://orcid.org/0000-0003-3998-4118
Huang-Ge Zhang https://orcid.org/0000-0001-9665-9202

REFERENCES
Akbay, E. A., Koyama, S., Liu, Y., Dries, R., Bufe, L. E., Silkes, M., Alam, M. M., Magee, D. M., Jones, R., Jinushi, M., Kulkarni, M., Carretero, J., Wang, X., Warner-Hatten, T., Cavanaugh, J. D., Osa, A., Kumanogoh, A., Freeman, G. J., … Wong, K. K. (2017). Interleukin-17A promotes lung tumor progression through neutrophil attraction to tumor sites and mediating resistance to PD-1 blockade. *Journal of thoracic oncology*, *12*(8), 1268–1279.

Lawrenz, Au - B. M., Au - Fodah, R. A., Au - Gutierrez, M. G., & Au - Warawa, J. (2014). Intubation-mediated intratracheal (IMIT) instillation: A noninvasive, lung-specific delivery system. *J. Vis. Exp.*, *93*, e52261.

Bazan-Socha, S., Kuczia, P., Potaczek, D. P., Mastalerz, L., Cybulska, A., Zareba, L., Kremers, R., Hemker, C., & Undas, A. (2018). Increased blood levels of cellular fibronectin in asthma: Relation to the asthma severity, inflammation, and prothrombotic blood alterations. *Respiratory Medicine*, *141*, 64–71.

Belda-Iniesta, C., Ibáñez de Cáceres, I., Barriuso, J., de Castro Carpeño, J., González Barón, M., & Feliú, J. (2008). Molecular biology of pancreatic cancer. *Clinical & translational oncology*, *10*(9), 530–537.

Bhusal, N., Lee, M., Lee, H., Adhikari, A., Han, A. R., Han, A., & Kim, H. S. (2021). Evaluation of morphological, physiological, and biochemical traits for assessing drought resistance in eleven tree species. *Science of the Total Environment*, *779*, 146466.

Buzas, E. I., György, B., Nagy, G., Falus, A., & Gay, S. (2014). Emerging role of extracellular vesicles in inflammatory diseases. *Nat Rev Rheumatol*, *10*(6), 356–364.

Cai, T., Qiu, J., Ji, Y., Li, W., Ding, Z., Suo, C., Chang, J., Wang, J., He, R., Qian, Y., Guo, X., Zhou, L., Sheng, H., Shen, L., & Qiu, J. (2019). IL-17-producing ST2(+) group 2 innate lymphoid cells play a pathogenic role in lung inflammation. *Journal of Allergy and Clinical Immunology*, *143*(1), 229–244.e229.

Dehghani, M., Gulvin, S. M., Flax, J., & Gaborski, T. R. (2020). Systematic evaluation of PKH labelling on extracellular vesicle size by nanoparticle tracking analysis. *Scientific Reports*, *10*(1), 9533.

Beckler, D., M., Higginbotham, J. N., Franklin, J. L., Ham, A. J., Halvey, P. J., Imasuen, I. E., Whitwell, C., Li, M., Liebler, D. C., & Coffey, R. J. (2013). Proteomic analysis of exosomes from mutant KRAS colon cancer cells identifies intercellular transfer of mutant KRAS. *Molecular & Cellular Proteomics*, *12*(2), 343–355.

Deng, Y., Gam, J., French, J. B., Zhao, H., An, S., & Benkovic, S. J. (2012). Mapping protein-protein proximity in the purinosome. *Journal of Biological Chemistry*, *287*(43), 36201–36207.

Dhiman, N., Sarvaiya, J., & Mohindroo, P. (2022). A drift on liposomes to proliposomes: Recent advances and promising approaches. *Journal of Liposome Research*, *32*(4), 317–331.

Hagner, M., Albrecht, M., Guerra, M., Braubach, P., Halle, O., Zhou-Suckow, Z., Butz, S., Jonigk, D., Hansen, G., Schultz, C., Dittrich, A. M., & Mall, M. A. (2021). IL-17A from innate and adaptive lymphocytes contributes to inflammation and damage in cystic fibrosis lung disease. *European Respiratory Journal*, *57*(6), 1–14.

Hamsten, C., Wiklundh, E., Grönlund, H., Schwenk, J. M., Uhlén, M., Eklund, A., Nilsson, P., Grunewald, J., & Häggmark-Månberg, A. (2016). Elevated levels of FN1 and CCL2 in bronchoalveolar lavage fluid from sarcoidosis patients. *Respiratory Research*, *17*(69), 1–14.

Jaeger, A. M., Stopfer, L. E., Ahn, R., Sanders, E. A., Sandel, D. A., Freed-Pastor, W. A., Rideout, W. M. 3rd, Naranjo, S., Fessenden, T., Nguyen, K. B., Winter, P. S., Kohn, R. E., Westcott, P. M. K., Schenkel, J. M., Shanahan, S. L., Shalek, A. K., Spranger, S., White, F. M., & Jacks, T. (2022). Deciphering the immunopeptidome in vivo reveals new tumour antigens. *Nature*, *607*(7917), 149–155.

Kalluri, R., & LeBleu, V. S. (2020). The biology, function, and biomedical applications of exosomes. *Science*, *367*(6478), 1–14.

Kharaziha, P., Ceder, S., Li, Q., & Panaretakis, T. (2012). Tumor cell-derived exosomes: A message in a bottle. *Biochimica Et Biophysica Acta*, *1826*(1), 103–111.

Kim, D. I., Birendra, K. C., Zhu, W., Motamedchaboki, K., Doye, V., & Roux, K. J. (2014). Probing nuclear pore complex architecture with proximity-dependent biotinylation. *PNAS*, *111*(24), E2453–2461.

Kuen, D. - S., Kim, B. - S., & Chung, Y. (2020). IL-17-producing cells in tumor immunity: Friends or foes? *Immune Network*, *20*(1), e6.

Kumar, A., Sundaram, K., Mu, J., Dryden, G. W., Sriwastva, M. K., Lei, C., Zhang, L., Qiu, X., Xu, F., Yan, J., Zhang, X., Park, J. W., Merchant, M. L., Bohler, H. C. L., Wang, B., Zhang, S., Qin, C., Xu, Z., … Zhang, H. G. (2021). High-fat diet-induced upregulation of exosomal phosphatidylcholine contributes to insulin resistance. *Nature Communications*, *12*(1), 213.

Larochelle, M., Bergeron, D., Arcand, B., & Bachand, F. (2019). Proximity-dependent biotinylation mediated by TurboID to identify protein-protein interaction networks in yeast. *Journal of Cell Science*, *132*(11), 1–14.

Liu, Q., Zheng, J., Sun, W., Huo, Y., Zhang, L., Hao, P., Wang, H., & Zhuang, M. (2018). A proximity-tagging system to identify membrane protein-protein interactions. *Nature Methods*, *15*(9), 715–722.

Lobb, R. J., Becker, M., Wen, S. W., Wong, C. S., Wiegmans, A. P., Leimgruber, A., & Moller, A. (2015). Optimized exosome isolation protocol for cell culture supernatant and human plasma. *J Extracell Vesicles*, *4*, 27031.

Masyuk, A. I., Masyuk, T. V., & Larusso, N. F. (2013). Exosomes in the pathogenesis, diagnostics and therapeutics of liver diseases. *Journal of Hepatology*, *59*(3), 621–625.

Moreau, P., Bessoule, J. J., Mongrand, S., Testet, E., Vincent, P., & Cassagne, C. (1998). Lipid trafficking in plant cells. *Progress in Lipid Research*, *37*(6), 371–391.

Mu, J., Zhuang, X., Wang, Q., Jiang, H., Deng, Z. B., Wang, B., Zhang, L., Kakar, S., Jun, Y., Miller, D., & Zhang, H. G. (2014). Interspecies communication between plant and mouse gut host cells through edible plant derived exosome-like nanoparticles. *Molecular Nutrition & Food Research*, *58*(7), 1561–1573.

Muñoz-Maldonado, C., Zimmer, Y., & Medová, M. (2019). A comparative analysis of individual RAS mutations in cancer biology. *Frontiers in oncology*, *9*, 1088.

Nikitin, A. Y., Alcaraz, A., Anver, M. R., Bronson, R. T., Cardiff, R. D., Dixon, D., Fraire, A. E., Gabrielson, E. W., Gunning, W. T., Haines, D. C., Kaufman, M. H., Linnoila, R. I., Maronpot, R. R., Rabson, A. S., Reddick, R. L., Rehm, S., Rozengurt, N., Schuller, H. M., Shmidt, E. N., … Jacks, T. (2004). Classification of proliferative pulmonary lesions of the mouse: recommendations of the mouse models of human cancers consortium. *Cancer Research*, *64*(7), 2307–2316.

Niu, Y., & Xiang, Y. (2018). An overview of biomembrane functions in plant responses to high-temperature stress. *Frontiers in Plant Science*, *9*, 915.

Piva, S., Ganzinelli, M., Garassino, M. C., Caiola, E., Farina, G., Broggini, M., & Marabese, M. (2014). Across the universe of K-RAS mutations in non-small-cell-lung cancer. *Current Pharmaceutical Design*, *20*(24), 3933–3943.

Roux, K. J., Kim, D. I., & Burke, B. (2013). BioID: a screen for protein-protein interactions. *Curr Protoc Protein Sci*, *74*, 19.23.11–19.23.14.

Roux, K. J., Kim, D. I., Raida, M., & Burke, B. (2012). A promiscuous biotin ligase fusion protein identifies proximal and interacting proteins in mammalian cells. *Journal of Cell Biology*, *196*(6), 801–810.

Salazar, Y., Zheng, X., Brunn, D., Raifer, H., Picard, F., Zhang, Y., Winter, H., Guenther, S., Weigert, A., Weigmann, B., Dumoutier, L., Renauld, J. C., Waisman, A., Schmall, A., Tufman, A., Fink, L., Brüne, B., Bopp, T., Grimminger, F., … Savai, R. (2020). Microenvironmental Th9 and Th17 lymphocytes induce metastatic spreading in lung cancer. *Journal of Clinical Investigation*, *130*(7), 3560–3575.

Sani, M. A., Tavassoli, M., Azizi-Lalabadi, M., Mohammadi, K., & McClements, D. J. (2022). Nano-enabled plant-based colloidal delivery systems for bioactive agents in foods: Design, formulation, and application. *Advances in Colloid and Interface Science*, *305*, 102709.

Schwanz, P., & Polle, A. (2001). Differential stress responses of antioxidative systems to drought in pendunculate oak (Quercus robur) and maritime pine (Pinus pinaster) grown under high CO(2) concentrations. *Journal of Experimental Botany*, *52*(354), 133–143.

Sears, R. M., May, D. G., & Roux, K. J. (2019). BioID as a tool for protein-proximity labeling in living cells. *Methods in Molecular Biology*, *2012*, 299–313.

Sheikholeslami, B., Lam, N. W., Dua, K., & Haghi, M. (2022). Exploring the impact of physicochemical properties of liposomal formulations on their in vivo fate. *Life Sciences*, *300*, 120574.

Sriwastva, M. K., Deng, Z. B., Wang, B., Teng, Y., Kumar, A., Sundaram, K., Mu, J., Lei, C., Dryden, G. W., Xu, F., Zhang, L., Yan, J., Zhang, X., Park, J. W., Merchant, M. L., Egilmez, N. K., & Zhang, H. G. (2022). Exosome-like nanoparticles from Mulberry bark prevent DSS-induced colitis via the AhR/COPS8 pathway. *Embo Reports*, *23*(3), e53365.

Takács, T., Kudlik, G., Kurilla, A., Szeder, B., Buday, L., & Vas, V. (2020). The effects of mutant Ras proteins on the cell signalome. *Cancer and Metastasis Reviews*, *39*, 1–14.

Teng, Y., Ren, Y., Sayed, M., Hu, X., Lei, C., Kumar, A., Hutchins, E., Mu, J., Deng, Z., Luo, C., Sundaram, K., Sriwastva, M. K., Zhang, L., Hsieh, M., Reiman, R., Haribabu, B., Yan, J., Jala, V. R., Miller, D. M., … Zhang, H. - G. (2018). Plant-derived exosomal microRNAs shape the gut microbiota. *Cell Host & Microbe*, *24*(5), 637–652.e8. http://www.sciencedirect.com/science/article/pii/S1931312818305237

Teng, Y., Xu, F., Zhang, X., Mu, J., Sayed, M., Hu, X., Lei, C., Sriwastva, M., Kumar, A., Sundaram, K., Zhang, L., Park, J. W., Chen, S. Y., Zhang, S., Yan, J., Merchant, M. L., Zhang, X., McClain, C. J., Wolfe, J. K., … Zhang, H. G. (2021). Plant-derived exosomal microRNAs inhibit lung inflammation induced by exosomes SARS-CoV-2 Nsp12. *Molecular Therapy*, *29*(8), 2424–2440.

To, T. L., Fadul, M. J., & Shu, X. (2014). Singlet oxygen triplet energy transfer-based imaging technology for mapping protein-protein proximity in intact cells. *Nature Communications*, *5*, 4072.

Wang, J., Deng, L., Huang, J., Cai, R., Zhu, X., Liu, F., Wang, Q., Zhang, J., & Zheng, Y. (2017). High expression of Fibronectin 1 suppresses apoptosis through the NF-κB pathway and is associated with migration in nasopharyngeal carcinoma. *American journal of translational research*, *9*(10), 4502–4511.

Wang, K., Kim, M. K., Di Caro, G., Wong, J., Shalapour, S., Wan, J., Zhang, W., Zhong, Z., Sanchez-Lopez, E., Wu, L. W., Taniguchi, K., Feng, Y., Fearon, E., Grivennikov, S. I., & Karin, M. (2014). Interleukin-17 receptor a signaling in transformed enterocytes promotes early colorectal tumorigenesis. *Immunity*, *41*(6), 1052–1063.

Wang, R., Yang, L., Zhang, C., Wang, R., Zhang, Z., He, Q., Chen, X., Zhang, B., Qin, Z., Wang, L., & Zhang, Y. (2018). Th17 cell-derived IL-17A promoted tumor progression via STAT3/NF-κB/Notch1 signaling in non-small cell lung cancer. *Oncoimmunology*, *7*(11), e1461303.

Waninger, J. J., Beyett, T. S., Gadkari, V. V., Siebenaler, R. F., Kenum, C., Shankar, S., Ruotolo, B. T., Chinnaiyan, A. M., & Tesmer, J. J. G. (2022). Biochemical characterization of the interaction between KRAS and Argonaute 2. *Biochem Biophys Rep*, *29*, 101191.

Wu, F., Xu, J., Huang, Q., Han, J., Duan, L., Fan, J., Lv, Z., Guo, M., Hu, G., Chen, L., Zhang, S., Tao, X., Ma, W., & Jin, Y. (2016). The role of interleukin-17 in lung cancer. *Mediators of Inflammation*, 8494079.

Xu, S., & Cao, X. (2010). Interleukin-17 and its expanding biological functions. *Cellular & Molecular Immunology*, *7*, 164–174.

Zhang, H., Dong, J., Zhao, X., Zhang, Y., Ren, J., Xing, L., Jiang, C., Wang, X., Wang, J., Zhao, S., & Yu, H. (2019). Research progress in membrane lipid metabolism and molecular mechanism in peanut cold tolerance. *Frontiers in Plant Science*, *10*, 838.

Zheng, S., Sieder, M., Mitterer, M., Reth, M., Cavallari, M., & Yang, J. (2019). A new branched proximity hybridization assay for the quantification of nanoscale protein-protein proximity. *Plos Biology*, *17*(12), e3000569.

Zheng, Y., Ding, L., Meng, X., Potter, M., Kearney, A. L., Zhang, J., Sun, J., James, D. E., Yang, G., & Zhou, C. (2022). Structural insights into Ras regulation by SIN1. *PNAS*, *119*(19), e2119990119.

Zhou, W. H., Du, W. D., Li, Y. F., Al-Aroomi, M. A., Yan, C., Wang, Y., Zhang, Z. Y., Liu, F. Y., & Sun, C. F. (2022). The overexpression of fibronectin 1 promotes cancer progression and associated with M2 macrophages polarization in head and neck squamous cell carcinoma patients. *Int J Gen Med*, *15*, 5027–5042.

Zhu, G., Pei, L., Xia, H., Tang, Q., & Bi, F. (2021). Role of oncogenic KRAS in the prognosis, diagnosis and treatment of colorectal cancer. *Molecular cancer*, *20*(1), 143.

SUPPORTING INFORMATION

Additional supporting information can be found online in the Supporting Information section at the end of this article.

How to cite this article: Sriwastva, M. K., Teng, Y., Mu, J., Xu, F., Kumar, A., Sundaram, K., Malhotra, R. K., Xu, Q., Hood, J. L., Zhang, L., Yan, J., Merchant, M. L., Park, J. W., Dryden, G. W., Egilmez, N. K., & Zhang, H.-G. (2023). An extracellular vesicular mutant KRAS-associated protein complex promotes lung inflammation and tumor growth. *Journal of Extracellular Vesicles*, *12,* e12307. https://doi.org/10.1002/jev2.12307